IOP Conf. Series: Journal of Physics: Conf. Series **880** (2017) 012036 doi:10.1088/1742-6596/880/1/012036

Measurements of entanglement over a kilometric distance to test superluminal models of Quantum Mechanics: preliminary results.

B Cocciaro, S Faetti and L Fronzoni

Department of Physics Enrico Fermi, Largo Pontecorvo 3, I-56127 Pisa, Italy

E-mail: b.cocciaro@comeg.it, sandro.faetti@unipi.it, leone.fronzoni@unipi.it

Abstract. As shown in the *EPR* paper (Einstein, Podolsky e Rosen, 1935), Quantum Mechanics is a non-local Theory. The Bell theorem and the successive experiments ruled out the possibility of explaining quantum correlations using only local hidden variables models. Some authors suggested that quantum correlations could be due to superluminal communications that propagate isotropically with velocity $v_t > c$ in a preferred reference frame. For finite values of v_t and in some special cases, Quantum Mechanics and superluminal models lead to different predictions. So far, no deviations from the predictions of Quantum Mechanics have been detected and only lower bounds for the superluminal velocities v_t have been established. Here we describe a new experiment that increases the maximum detectable superluminal velocities and we give some preliminary results.

1. Introduction

The non local character of Quantum Mechanics (QM) has been object of a great debate starting from the famous Einstein-Podolsky-Rosen (EPR) paper [1]. Consider, for instance, a quantum system made by two photons a and b that are in the polarization entangled state

$$|\psi >= \frac{1}{\sqrt{2}} \left(|H, H > + e^{i\phi} |V, V > \right) \tag{1}$$

where H and V stand for horizontal and vertical polarization, respectively, and ϕ is a constant phase coefficient. The two entangled photons are created at point O, propagate in space far away one from the other (see Fig.1) and reach at the same time points A (Alice) and B (Bob) that are equidistant from O as schematically drawn in Fig.1. Two polarizing filters P_A and P_B lie at points A and B, respectively.

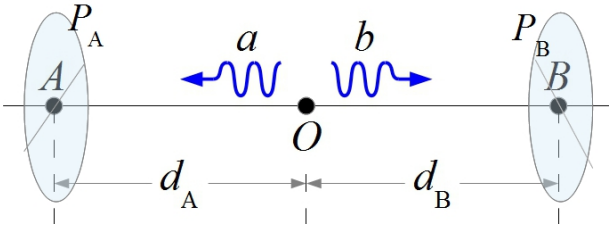

Figure 1: O: source of entangled photons (a and b); A(Alice) and B(Bob): points equidistant from O ($d_A = d_B$); P_A and P_B: Polarizing filters centered at points A and B, respectively.

IOP Conf. Series: Journal of Physics: Conf. Series **880** (2017) 012036 doi:10.1088/1742-6596/880/1/012036

Suppose, now, that the polarizers axes are aligned along the horizontal direction. According to *QM*, the passage of photon a (or b) through polarizer P_A (or P_B) leads to the collapse of the entangled state to $|H,H>$ everywhere, then, also photon b (or a) collapses to the horizontal polarization. This behaviour suggests the existence of a sort of "action at a distance" between entangled particles in complete disagreement with any other classical physic phenomenon (Electromagnetism , Gravity ....). According to Gisin [2, 3], classical correlations between far events have always due to two possible mechanisms: Common Cause or Communications. The Bell theorem[4] and many successive *EPR* experiments[5–14] demonstrated that correlations cannot be due only to a common cause (*hidden variables theories*) or to common cause + subluminal communications. According to Bell, "*in these EPR experiments there is the suggestion that behind the scenes something is going faster than light*"[15]. Models of *QM* based on the presence of superluminal communications (tachyons) have been proposed [16, 17]. Tachyons are known to lead to causal paradoxes (see, for instance, pages 52-53 in [18]), but no causal paradox arises if tachyons propagate isotropically in a preferred frame (PF) with velocity $v_t = \beta_t c$ ($\beta_t > 1$)[19–23].

Suppose, now, that quantum correlations are due to superluminal communications and that an *ideal experiment* is performed in the tachyon preferred frame S' where two polarizing filters lie at the same optical distances $d'_A = d'_B$ from source O. Photons a and b get the polarizers at the same time and no communication is possible. Then, correlations between entangled particles should differ from the predictions of *QM* and should satisfy the Bell inequality. However, from the experimental point of view, equality $d'_A = d'_B$ can be only approximatively verified within a given uncertainty $\Delta d'$. Consequently, photons a and b could get the polarisers at two different times ($\Delta t' = {}^{\Delta d'}/_{c}$) and could communicate if the tachyon velocity exceeds a lower bound $v_{t,min} = c\,(d'_{AB}/\Delta d')$ where d'_{AB} is the distance between polarizers P_A and P_B in the PF. Two are the possible experimental results: *i)* a lack of quantum correlations is observed; *ii)* quantum correlations are always satisfied. In the first case (*i)*) one should conclude that quantum correlations are due to exchange of superluminal messages with velocity lower than $v_{t,min}$. In the second case (*ii)*), due to the experimental uncertainty $\Delta d'$, one cannot invalidate the superluminal model of *QM* but can only establish a lower bound $v_{t,min} = c\,(d'_{AB}/\Delta d')$ for the superluminal velocities. It has been recently demonstrated an important theorem [24, 25]: if *QM* correlations are due to superluminal signals with finite velocity v_t, then also a *macroscopic superluminal signalling* becomes possible provided that states of three or four entangled particles are involved. This means that the superluminal signals do not remain hidden but they could lead to macroscopic superluminal communications. In conclusion, there are two possible alternative situations both involving some upheaval of the common thought: *a*) Nature is intrinsically non local and far events can be correlated without any common cause or communication (orthodox *QM*); *b*) Nature is local but, in this case, macroscopic superluminal signalling is possible (superluminal models). Physics is an experimental Science and, thus, we think that only the experiments can decide between these two alternatives.

The correlations between entangled particles can be experimentally tested measuring the number of coincidences $N(\alpha_A, \alpha_B)$ of photons passing through polarizers P_A and P_B for different values of the polarizers angles α_A and α_B with respect to the horizontal axis. In particular, two correlations parameters S_{max} and S_{min} can be measured (see equations (33) and (34) in reference [26]):

$$S_{max} = \frac{N(45°,67.5°)\text{- }N(0°,67.5°)\text{ - }N(45°,112,5°)\text{ - }N(90°,22.5°)}{N} \tag{2}$$

and

$$S_{min} = \frac{N(135°,202.5°)\text{- }N(0°,202.5°)\text{ -}N(135°,157,5°)\text{ - }N(90°,67.5°)}{N}, \tag{3}$$

where N is the number of coincidences with no polarizers (tacking into account for the polarizers transmission) that can be written as:

$$N = N(0°,0°)+N(0°,90°)+N(90°,0°)+N(90°,90°) \tag{4}$$

Eqs. (2), (3) and 4 have been obtained from equation (33) in reference [26] using the equalities:

$$\begin{array}{l} N(a',\infty) = N(a',b) + N\left(a',b+90°\right) \\ N(\infty,b) = N(a,b) + N\left(a+90°,b\right) \end{array} \tag{5}$$

Quantum Mechanics predicts $S_{max} = 0.207$ and $S_{min} =$ - 1.207, respectively, whilst local theories must satisfy the inequalities $S_{max} \leq 0$ and $S_{min} \geq$ -1. Then, the measurement of one of these parameters makes possible a direct test of the superluminal models.

So far we considered an ideal experiment performed in the preferred frame, but the *PF* is unknown. A more complex *EPR* experiment can be still performed in the Earth if A and B are aligned along the Est-West axis and are equidistant (in the Earth frame) from the photons source at O. Of course, the entangled photons get simultaneously polarizers P_A and P_B in the Earth reference frame but not in the *PF*. However, according to Relativity, these events become simultaneous also in the *PF* if the velocity vector $\vec{V} = \vec{\beta}c$ of the *PF* is orthogonal to the A-B axis (see, for instance, the appendix in[27]). If the A-B axis coincides with the East-West direction, due to the Earth rotation around its axis, there are always two times t_1 and t_2 during each sidereal day where vector $\vec{V}$ becomes orthogonal to the A-B axis. If the A-B axis makes an angle $\gamma \neq 0$ with the Est-West axis, vector $\vec{V}$ becomes orthogonal to the A-B axis only if angle θ between vector $\vec{V}$ and the Earth polar axis lies in the interval $[\gamma, \pi - \gamma\ ]$. If this condition is satisfied, a loss of Quantum correlations should be observed at two given unknown times t_1 and t_2 each day if the tachyon velocity v_t is lower than the maximum detectable velocity $v_{t,min}$. However, there is an other important feature that can reduce the maximum detectable tachyons velocities in the Earth experiment. In fact, tachyons get simultaneously the polarizers also in the *PF* only at the two well defined times t_1 and t_2 but the measure of the coincidences numbers $N(\alpha_A, \alpha_B)$ is not instantaneous and requires a finite acquisition time δt. This produces a further uncertainty on the equalization of the optical paths that is an increasing function of the acquisition time and the reduced velocity β of the *PF*. Using the Relativity theory, it has been shown [28, 29] that the lower limit of the detectable tachyon velocities in a Earth experiment is:

$$\beta_{t,min} = \sqrt{1 + \frac{(1-\beta^2)\left[1-\bar{\rho}^2\right]}{\left[\bar{\rho} + \beta \sin\chi \sin\frac{\pi\delta t}{T}\right]^2}}, \tag{6}$$

where $\bar{\rho} = {}^{\Delta d}/_{d_{AB}}$, Δd is the uncertainty on the equalization of the optical paths in the Earth frame, T is the duration of the sidereal day, δt is the acquisition time, χ is the polar angle between the North-South axis and velocity $\vec{V}$ of the *PF* and β is the reduced *PF* velocity ($\beta = {}^{V}/_{c}$). In typical experimental conditions [28–30], the acquisition time δt is much smaller than the sidereal day T and $\beta_{t,min}$ is a decreasing function of both $\bar{\rho}$ and δt that reaches a minimum value if $\chi = {}^{\pi}/_{2}$. $\beta_{t,min}$ is also a decreasing function of β that assumes its maximum value $\beta_{t,min} = \frac{1}{\bar{\rho}}$ for $\beta = 0$ and approaches the minimum value $\beta_{t,min} = 1$ for $\beta \to 1$. Our following considerations and figures will be restricted to $\delta t \ll T$ and to the most unfavourable condition $\chi = {}^{\pi}/_{2}$. The typical plot of function $\beta_{t,min}$ versus the reduced velocity β of the *PF* for $\chi = {}^{\pi}/_{2}$ and for some values of $\bar{\rho}$ and δt is drawn in Fig.2.

Experiments of this kind have been performed by some groups in the last years[28–30]. In all these experiments no loss of *QM* correlations has been observed and, thus, only lower bounds $\beta_{t,min}$ for the tachyons reduced velocities have been established. Recently[27] we proposed a new experiment to increase the maximum detectable tachyons velocities by about two orders of

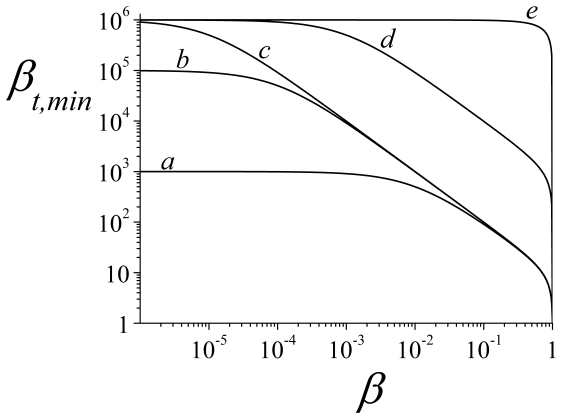

Figure 2: Function $\beta_{t,min}$ versus β for the unfavourable case $\chi = \pi/2$ and for some values of the experimental parameters $\bar{\rho}$ and δt. Curves a, b and c correspond to the fixed acquisition time $\delta t = 10^{-1} \times \frac{T}{\pi}$ and to decreasing values of $\bar{\rho}$ ($a : \bar{\rho} = 10^{-3}$, $b : \bar{\rho} = 10^{-5}$, $c : \bar{\rho} = 10^{-6}$). Curves c, d and e correspond to a fixed value $\bar{\rho} = 10^{-6}$ and to decreasing values of δt ($c : \delta t = 10^{-1} \times \frac{T}{\pi}$, $d : \delta t = 10^{-3} \times \frac{T}{\pi}$, $e : \delta t = 10^{-7} \times \frac{T}{\pi}$).

magnitude. Here we describe our improved experimental apparatus and we report some very preliminary experimental results. The main features of the experiment are discussed in Section 2. The preliminary experimental results are in Section 3, whilst the conclusions are in Section 4.

2. The experimental apparatus and the main sources of error.

2.1. Production and detection of entangled photons.

The main goal of our experiment is to make parameters $\bar{\rho} = {}^{\Delta d}/_{d_{AB}}$ and δt as smaller as possible to increase the lower bound $\beta_{t,min}$. Small values of $\bar{\rho} = {}^{\Delta d}/_{d_{AB}}$ ($\bar{\rho} \approx 1.8 \times 10^{-7}$) are obtained using a large distance d_{AB} ($d_{AB} = 1200\,\mathrm{m}$) and a small uncertainty Δd ($\Delta d < 220\,\mu\mathrm{m}$). A high intensity source of entangled photons provides a high coincidences rate (15000 coinc/s) and, thus, a small minimum acquisition time that is estimated to be $\delta t \approx 0.1\,\mathrm{s}$. The experiment is performed in the "East-West" gallery of the European Gravitational Observatory (EGO) of Cascina that hosts the $VIRGO$ experiment on the detection of gravitational waves[31]. Unfortunately, this gallery makes an angle $\gamma = 18°$ with the actual East-West axis. Then, vector $\vec{V}$ becomes orthogonal to the gallery axis at two times t_1 and t_2 only if angle θ between vector $\vec{V}$ and the Earth polar axis lies in the interval $[\gamma, \pi - \gamma]$. This means that we do not look at the entire celestial sphere but only at a $\approx 95\%$ fraction of it. In fact, the excluded solid angle is $\Omega = 2\int_0^{\gamma} 2\pi \sin\theta d\theta \approx 5\%$ of the 4π total solid angle.

The experimental apparatus is schematically shown in figure 3. A 220 mW diode laser beam ($\lambda = 406.5\,\mathrm{nm}$) is polarized (polariser P_0) and the polarization axis can be rotated by a motorized $\lambda/2$ plate. All the measurements reported in this paper have been performed with the polarization axis making a 45° angle with the horizontal axis. The beam passes through a Babinet-Soleil compensator and impinges at normal incidence on two thin (0.56 mm) adjacent non-linear optical crystals (BBO) cut for type-I phase matching [32]. The beam is focused on the BBO plates with the beam waist having a 0.6 mm diameter. The optic axes of the BBO plates are tilted at the angle 29.05° and lie in planes perpendicular to each other with the first plane that is horizontal. The pump beam induces down conversion at the wavelength $\lambda = 813\,\mathrm{nm}$ in each crystal[32] with maximum emission at the two symmetric angles $\gamma_A = -\gamma_B = 2.42°$ with respect to the pump laser beam. Suitable optical diaphragms select the entangled beams that are emitted within cones of aperture 0.8° centred at the maximum emission angles. The down converted photons are created in the maximally entangled state $\left(|H,H> + e^{i\phi}|V,V>\right)/\sqrt{2}$, where phase ϕ can be changed moving the motorized Babinet-Soleil compensator. Plates C , C_A and C_B in figure 3 are suitable compensating plates that provide a compensation of spurious effects due to the poor coherence of the pump beam (C) and to the anisotropy of the BBO

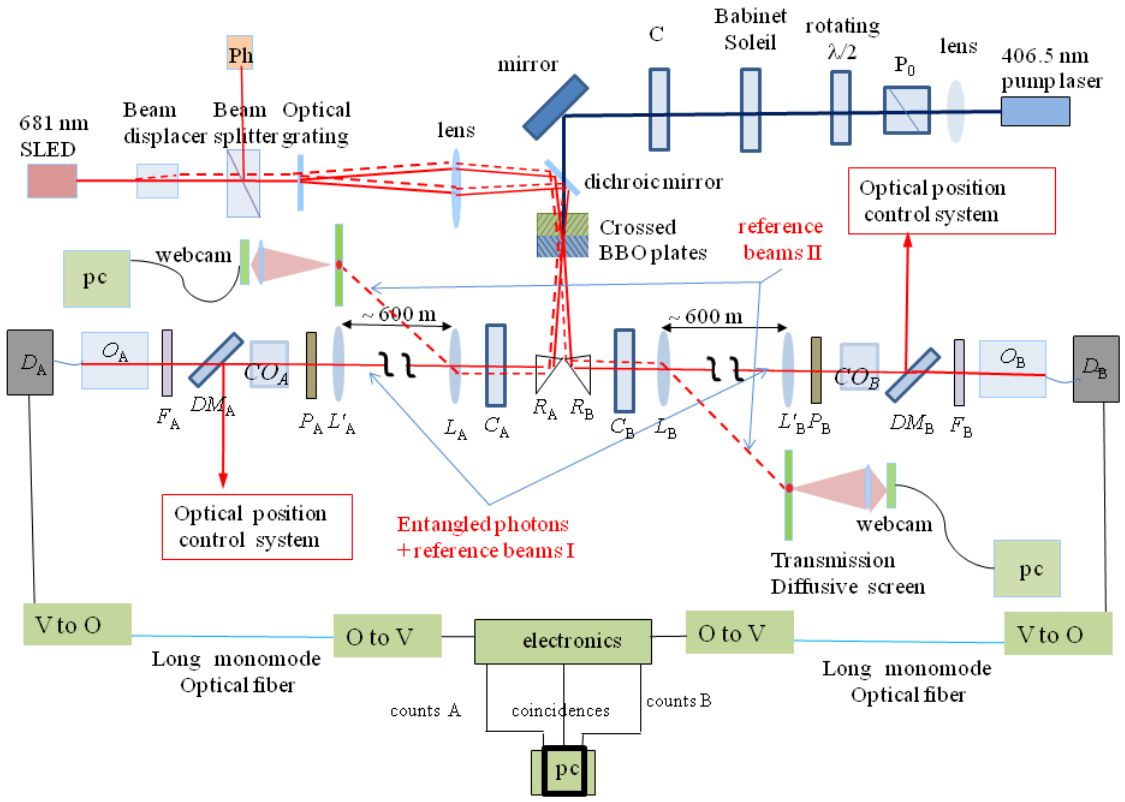

Figure 3: Schematic view of the experimental apparatus. To simplify the drawing some details that will be discussed below have not be inserted in the figure. The pump beam (blue in the figure) is polarized by the polarizer P_0 and the $\lambda/2$ plate. The Babinet-Soleil compensator introduces a variable optical dephasing between the horizontal and vertical polarizations. C , C_A and C_B are anisotropic compensator plates used to increase the fidelity of the entangled state. The pump beam is focused on two adjacent BBO plates where the entangled photons are generated and emitted at the angles $\pm 2.42^{\circ}$ with respect to the pump laser beam. L_A, L_B, L'_A and L'_B are achromatic lenses aligned along the EGO gallery and having a 6 m focal length and a 15 cm diameter. Note that the figure is not to scale and, in particular, the distances between lenses L_A and L_B and L'_A and L'_B are very large (≈ 600 m). P_A and P_B are polarizing filters. O_A , O_B , CO_A and CO_B are systems of lenses. DM_A and DM_B are dichroic mirrors, F_A and F_B are optical filters, D_A and D_B are photon counting detectors. The superluminous diode ($SLED$), the beam displacer and the optical grating are used to produce two reference beams in each arm of the EGO gallery as discussed below (full and broken red lines). V to O denote electronic systems that transform the output voltage pulses produced by the photon counting detectors into optical pulses, whilst O to V transform the optical pulses into voltage pulses.

plates(C_A and C_B)[33–35]. With these compensating plates we obtain a high intensity source of entangled photons with high fidelity. All the components described above lie on a central optical table that is entirely enclosed in an insulating box. One of the lateral internal walls is made by a 50 cm × 150 cm aluminium plate (5 mm − thickness) in thermal contact with copper tube coils where a paraflu fluid circulates. Two 80 W fans inside the box move the air and homogenize the temperature everywhere. In this way, the internal temperature can be maintained fixed better than $\pm 0.1\,^{\circ}$C. Two couples of specially designed achromatic lenses L_A, L_B, L'_A and L'_B (diameter = 15 cm, focal length = 6 m) allow us to obtain two 1:1 images of the entangled photons source on two thin near infrared polarizing films ($LPNIR$, Thorlabs) P_A and P_B that

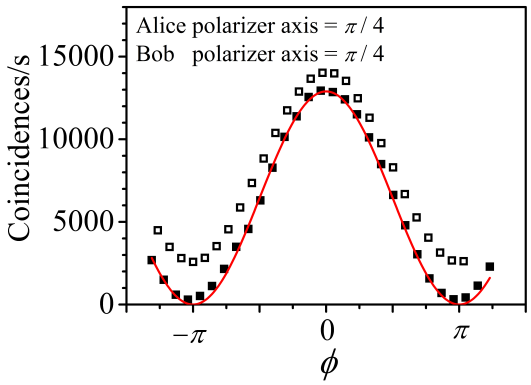

Figure 4: Dependence of the coincidences rate on phase ϕ when all the polarizers angles are fixed at 45 degrees. Full squares correspond to the experimental values with subctracted statistical coincidences. The open squares are the experimental results with subctracted statistical coincidences but whithout using the Kwiatt compensators C_A, C_B and C. The full line correspond to the prediction of Quantum mechanics for the entangled state of eq.(1).

lie at a 600 m distance from the source. The entangled photons pass through polarizers P_A and P_B and through the optical sets CO_A and CO_B that will be described below. Then, they are transmitted (98% transmission) by dichroic mirrors DM_A and DM_B (Chroma T760lpxr) and by two Chroma Techn. Corp. filtering sets F_A and F_B each composed by a bandpass filters ET810/40m ($\lambda = 810\,\text{nm} \pm 20\,\text{nm}$) and two low pass ET765lp filters ($\lambda_c = 765\,\text{nm}$). Finally, two identical optical lenses O_A and O_B focus the entangled photons on two Thorlabs multi mode optical fibres having a large diameter core ($200\,\mu$m) and high numerical aperture (0.39). The ends of fibres are connected to the inputs of the single photons counters D_A and D_B (Perkin Elmer SPCM-AQ4C) that generate output voltage pulses with a 25 ns width. The voltage pulses are transformed into optical pulses by LCM155EW4932-64 modules of Nortel Networks (V to O module in fig. 3) that propagate in single mode optical fibres up to the central optical table where they are converted into electric pulses (O to V module in fig.3) and sent to an electronic monostable circuit that provides output squared voltage pulses together with coincidences pulses. Before starting the measurements we have measured the light spectral absorption due to air and we have verified that the adsorption in the wavelengths interval [790 nm−830 nm] is essentially due to water vapour. The total adsorbed light in this interval is a fraction lower than 3% of the incident light for a 45% air relative humidity. The coincidence rate measured by counters versus phase ϕ is shown in figure 4. Note the satisfactory contrast of the fringes that is obtained using the Kwiat et al. compensating plates[33–35].

2.2. Compensation of the beam deflections.
An interferometric method is used to equalize the optical paths from the source of the entangled photons to polarizers P_A and P_B. The method exploits two reference beams (beams I in figure 3) of wavelength $\lambda = 681$ nm and coherence length $L_A = 28.1\,\mu$m produced by a super luminous diode (*SLED* in figure 3). Due to the occurrence of vertical temperature gradients up to 3 °C/m in the *EGO* gallery produced by sunlight, it has been needed to use two couples of different reference beams (beams I and II) in each arm of the interferometer. It can be easily shown that an uniform vertical temperature gradient generates a vertical gradient of the air refractive index that produces the same effect as a diffused optical prism leading to a continuous deviation of the optical beams I and II up to about 1 m at a 600 m distance.The full curve in Figure 5(b) shows the average trajectory of beam I when a vertical temperature gradient occurs. A parabolic shape of the trajectory is predicted if the vertical temperature gradient is everywhere constant in the gallery. Furthermore, the small non uniformity of the vertical gradient of the air refractive index simulates a diffused cylindrical lens that leads to astigmatism of the images.

The accurate compensation of these effects is needed to collect a great number of entangled photons on the photon counting detectors. Beam I follows the same optical path of the entangled

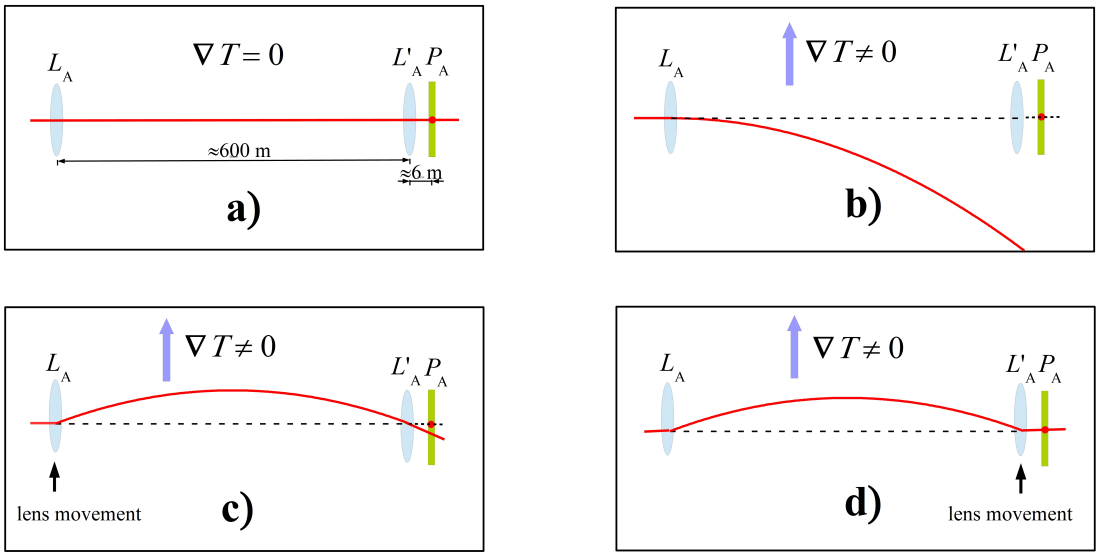

Figure 5: The average trajectory of beam I in an arm (the Alice arm) of the *EGO* gallery with and without vertical temperature gradient. The figure is not to scale but two characteristic dimensions are given in figure (a). (a): The vertical temperature gradient is not present: the average beam trajectory is a straight horizontal line and the beam impinges at the centre of polarizer P_A. (b) A vertical temperature gradient is present: the reference beam I exhibits a parabolic trajectory. (c) A suitable movement of lens L_A deviate the transmitted beam and leads to a new parabolic trajectory that passes through the centre of lens L'_A. Note that, now, the incidence angle of the beam on lens L'_A is not zero and the transmitted beam does not impinge at the centre of polarizer P_A. (d) A suitable movement of lens L'_A deviate the transmission beam toward the centre of polarizer P_A.

photons and provides an interferometric signal whilst beam II is horizontally displaced with respect to beam I and allows us to compensate the vertical deflections of the beams (up to 1 m at a 600 m distance) produced by the air refractive index gradients. The method to generate the reference beams has been greatly improved with respect to that proposed in [27]. Here we obtain the reference beams I and II using the beam displacer (Thorlabs BDY12U) in figure 3 to split the incident *SLED* beam into two parallel beams at a 1.2 mm horizontal distance. The two beams pass through a beam splitter and are focused on a transmission phase grating that produce +1 and -1 order diffracted beams with 35% intensity with respect to the incident beam and at the average diffraction angles $+2.43°$ and $-2.43°$ that are virtually coincident with the maximum emission angles of the entangled photons ($\pm 2.42°$). The beam waists of the two reference beams spots on the optical grating have a 0.3 mm diameter and behave as two sources localized on the grating at a 1.2 mm horizontal distance. The optical rays emitted by these sources at the angles $+2.43°$ and $-2.43°$ pass through an achromatic lens having a 150 mm focal length, are reflected by a 565 nm short pass dichroic mirror (Chroma T565spxe) and produce 1:1 images of the grating spots on the *BBO* plates. Using a suitable optical method, the image of the reference source I on the *BBO* plates is centred with respect to the spot of the pump beam where the entangled photons are generated. The procedure above ensures that the reference beams I outgoing from the *BBO* plates are initially in phase and are superimposed to the entangled photons. This provides the easy alignment of the optical apparatus and the control of the optical paths of the entangled photons. Achromatic lenses L_A, L_B, L'_A and L'_B have been

built to have the same 6000 mm focal length (within ±10 mm) for the pump laser and for the *SLED*. 1:1 images of the reference source I and of the entangled photons source are produced by lenses L_A, L_B, L'_A and L'_B on polarizers P_A and P_B at a 600 m distance from the source. Reference beams II are horizontally deflected by lenses L_A and L_B and produce two spots at a horizontal distance of 12 cm from the centres of lenses L'_A and L'_B on two diffusing screens horizontally adjacent to the lenses (see figure 3). Two optical objectives collect the diffused beams and produce images of the spots on two webcams. All lenses L_A, L_B, L'_A and L'_B can be moved horizontally and vertically using Sigma Koki *PC* controlled motors. A labview program measures the position of the beams spots on the webcams and produces feedback signals that move lenses L_A and L_B to maintain the spots positions fixed. In such a way also the reference beams I (and the entangled photons) always remain fixed at the centre of lenses L'_A and L'_B (see Figure 5(c)). A 1 cm movement of lenses L_A and L_B produces a 1 m displacement of the beams spots at a 600 m distance. The feedback procedure leads to a complete control of the slow drifts of the beams but it cannot eliminate the rapid changes of the beam trajectories occurring within a few seconds time. This leads to a residual fluctuation of the beam spots at the centres of lenses L'_A and L'_B that is lower than ±30 mm. These residual displacements are appreciably smaller than the radius of the lenses (75 mm), then all the entangled photons are collected by them. The beams impinge at the centres of lenses L'_A and L'_B but the incidence angles change with time, due to the vertical refractive index gradient. Then, the images of the source of beams I (and of the entangled photons) that occur on polarizers P_A and P_B do not remain fixed at the centre of the polarizers (see figure 5c)). To stabilize these images at the centre of the polarizers, the reference beams I transmitted by the polarizers pass through two systems of cylindrical lenses CO_A and CO_B, are reflected by the 760 nm long pass dichroic mirrors DM_A and DM_B (Chroma T760lpxr) and impinge on two optical position control systems. Each optical position control system produces two 1:1 images of the beam spots occurring on the polarizers: one image is collected by a position sensing detector (Thorlabs PDP90A) and the other by a webcam. Labview feedback programs read the output of the position sensing detectors and move lenses L'_A and L'_B to maintain fixed the position of the beam spots at the centre of the two polarizers (see Figure 5(d)). In this case, too, slow drifts are completely removed but not the rapid displacements of the spots from the polarizers centres. These latter residual fluctuations remain always restricted below ±0.4 mm. Other labview feedback programs acquire the images of the webcams and measure the astigmatism of the images induced by non uniformities of the refractive index gradients. Each system of cylindrical lenses CO_A and CO_B is composed by a fixed cylindrical lens and a movable cylindrical lens that provide an effective cylindrical lens with a variable focal length. Suitable feedback signals generated by the labview program move the motorized cylindrical lenses to correct the astigmatism of the images. These procedures ensure that the spots of the reference beams I remain virtually fixed at the centre of polarizers P_A and P_B with a circular shape having a ≈ 0.3 mm diameter. Two images of the spot of the reference beam on polarizer P_A are shown in figures 6a) and 6b). Figure 6a) shows the spot for moderate sunlight with feedback *OFF*, whilst figure 6b) shows the same image with feedback *ON*. It must be remarked that our method stabilizes the spots of the 681 nm reference beams but the wavelengths of the entangled photons (790 nm − 830 nm) are different from those of the sled beam. However, the differences of the air refractive indices corresponding to the reference beams and to the entangled photons are very small and it can be shown that also the spots of the entangled photons on the polarizers always remain very close to the centres of the polarizers within 0.4 mm. In conclusion, our compensation procedure maintains the spot of the entangled photons restricted to a circular region close to the centre of the polarizers with a small diameter (≈ 0.6 mm) and ensures that virtually all the entangled photons passing through the polarizers are collected by the photon counting detectors also in conditions of great sunlight.

Figure 6: (a): The beam spot of the reference beam I on polarizer P_A in conditions of moderate sunlight and with feedback *OFF*. (b): The same spot with feedback *ON*. The diameter of the circular spot in 6b) is 0.3 mm.

2.3. Equalization of the optical paths.
To equalize the optical paths we exploit the reflections of the reference beams I from polarizers P_A and P_B. The reflected beams come back on the same path forward and impinge at the angles $+2.43°$ and $-2.43°$ on the optical phase grating where diffraction occurs again. The output beams that are diffracted orthogonally to the grating are reflected by the beam splitter and impinge on photodetector *Ph* where interference occurs. Air density fluctuations inside the *EGO* gallery induce oscillations of the optical path difference and, thus, an oscillating output voltage of the photodetector. The variations of the optical path differences are always greater than the optical wavelength and the output voltage oscillates from a minimum value (destructive interference) toward a maximum value (constructive interference). The peak to peak amplitude V_{pp} is measured by a simple electronic circuit. V_{pp} is maximized when the path difference is zero whilst V_{pp} tends to vanish if the path difference becomes greater than the *SLED* coherence length $L_c = 28.1\,\mu$m. Polarizer P_B is moved by a precision linear motorized stage (Physik Instruments M-406.22s) that is controlled by a *PC* through a labview program that generates a sweep of the P_B position and acquires the corresponding V_{pp} values. The typical dependence of V_{pp} on the polarizer position x during a summer night is shown in figure 7 (a) whilst the dependence during a summer day at the maximum sunlight is shown in figure 7(b). Note that the curve in figure 7(b) has a two bells profile. This behaviour can be explained assuming that the path difference oscillates with time around the average value Δd_{av} with a mean oscillation amplitude A. In these conditions, the typical Gaussian behaviour due to the finite coherence length of the *SLED* is expected to split into two nearly Gaussian profiles at distance $2A$. The central point between the two Gaussian peaks corresponds to the position of polarizer P_B where the average optical path difference is zero whilst the semi-distance between the two Gaussian Maxima corresponds to the average amplitude A of the fluctuations of the paths difference. The Full lines in figures 7(a) and 7(b) are the labview best fits of the experimental results with two Gaussians having the width $w = 0.020\,$mm that characterizes the *SLED* source. From these best fits we deduce that the main amplitude of the oscillations of the path difference is smaller than $10\,\mu m$ during night but it becomes $33\,\mu m$ at the maximum sunlight.

The labview feedback program operates in this way: first of all a large amplitude sweep is made to localize the central point x_c between the two Gaussian, then the sweep amplitude is reduced to $200\,\mu m$ around x_c and the new x_c value is memorized and plotted. This latter procedure with a $200\,\mu m$ sweep is repeated continuously each 15 s for the entire measurement time (24 hours) and, thus, the difference between the optical paths remains restricted to $\Delta d = \pm 100\,\mu$m at each time. The time-dependence of x_c due to the temperature variations for an entire Summer day is shown in figure 8.

Note that the complete interference pattern is somewhat more complex than the small portion

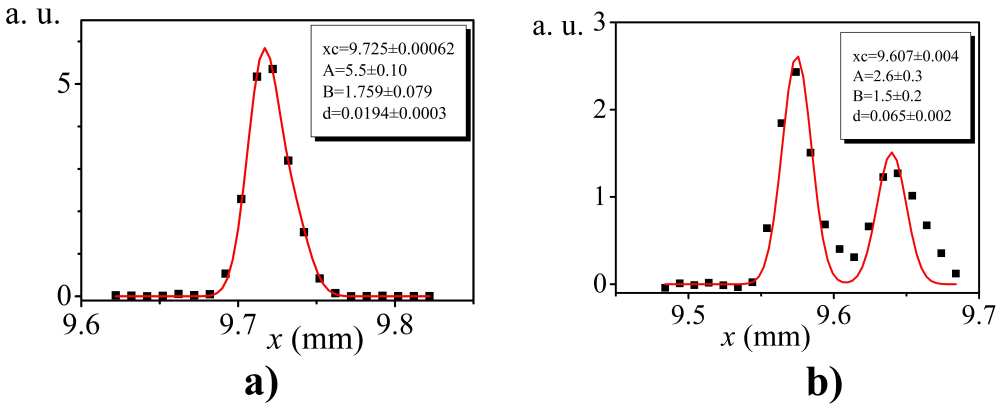

Figure 7: (a): The peak to peak of the output voltage of photodetector *Ph* during a Summer night versus the position x of the polarizer. Similar results are obtained in conditions of covered sky. The full line is the best fit with two slightly shiften Gaussian profiles $y = A\exp\left\{[(x-x_c-d/2)/w]^2\right\} + B\exp\left\{[(x-x_c+d/2)/w]^2\right\}$ where w is fixed to the value $w = 0.020\,\text{mm}$ that characterizes the *SLED* source and A, B,x_c and d are fitting parameters. x_c and d are measured in millimeters whilst A and B are in arbitrary unities. (b): The same dependence but in conditions of maximum sunligth. The two fitting Gaussians show a much greater separation due to the much greater amplitude of the optical paths fluctuations and the quality of the fit is poor due to noise effects induced by the strong air tourbolence.

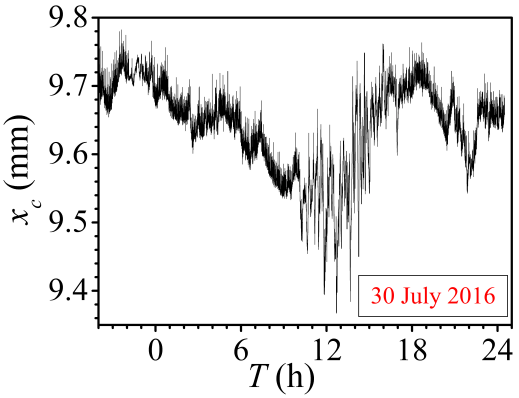

Figure 8: Variation of the equalization position x_c of the motorized polarizer during an entire Summer day. The maximum variation during the entire day is about 0.4 mm. Note the sharp and high amplitude variations due to the air turbulence during the maximum sunlight hours (from 10 h to 16 h).

shown in figures 7 since the *LPNIR* Thorlabs polarizers are made by a thin polarizing film ($280\,\mu$m thickness) sandwiched between two glass plates. We have measured with accuracy the thickness of the glasses and we have found that their values are $904\,\mu\text{m} \pm 5\,\mu\text{m}$. Due to the sandwich shape of the polarizers, there are many interfaces giving reflected beams that can interfere. Also in the optimal night conditions we observe five main interference peaks that are separated each from the other by a distance about 1.5 mm. After a careful analysis, the central peak has been clearly identified as that which corresponds to the equalization of optical paths from the source to the polarizing thin layers. Then, our analysis has been restricted only to the central peak region corresponding to figures 7.

As shown in Section 1, one of the most important parameters of our experiment is the uncertainty Δd on the equalization of the optical paths. Here we resume the main contributions to this uncertainty (see also[27]) :

a) the above described uncertainty due to the motor sweep $\Delta d_{sweep} = 100\,\mu$m that

corresponds to a half of the total sweep excursion,

b) the uncertainty Δd_{pol} due to the finite thickness ($280\,\mu m$) of the *LPNIR* Thorlabs polarizers layers. Since the extinction ratio of these polarizers at the entangled photons wavelengths is greater than 10^5, then we can estimate that 99% of photons with orthogonal polarization are adsorbed in a layer having a thickness $\approx 120\,\mu$m and we can assume the corresponding uncertainty value $\Delta d_{pol} = 120\,\mu$m.

c) The optical paths are equalized using the reference beams I that have not the same wavelength of the entangled photons. If the temperature would be uniform in the *EGO* gallery and the thickness of lenses L_A, L_B, L'_A and L'_B would be the same, also the entangled photons paths would be automatically equalized. This is no more true if there is a average temperature difference ΔT between the two arms of the interferometer or if there are differences between the thicknesses of the lenses. Calculations of these effects are somewhat complicate and need the knowledge of the temperature dependence of the refractive indices of the air and of the lenses at different wavelengths and the knowledge of the thickness differences between lenses L_A, L_B, L'_A and L'_B. The lenses thickness differences have been measured to be smaller than 0.1 mm and they do not affect appreciably the uncertainty. It results from the calculations that an average temperature difference $\Delta T = 1$°C between the two arms of the interferometer produces an optical paths difference slightly smaller than $10\,\mu$m. Since the horizontal temperature differences in the gallery are always smaller than 2-3 degrees, we get $\Delta d_{\Delta T} < 30\,\mu$m.

d) In our experiment we detect entangled photons with wavelengths from 790 nm toward 830 nm. Due to the optical dispersion, photons of different wavelengths see different optical paths in air and in the lenses, although this latter contribution is negligible. The difference of the optical paths due to the air optical dispertion is given by $\Delta d_{disp} = \frac{\partial n}{\partial \lambda}\Delta\lambda d$, where d is the distance from the source to polarizers (600 m) and $\Delta\lambda = 40$ nm is the bandwidth of the bandpass filters and n is the air refractive index. Substituting in the expression of Δd_{disp} the value $\frac{\partial n}{\partial \lambda} = 5.87 \times 10^{-9} nm^{-1}$ calculated using the Ciddor equation [36] at room conditions and with humidity = 50% and $CO_2 = 450$ micromol/mol, we get $\Delta d_{disp} = 144\ \mu m$. The resulting uncertainty in the optical paths differences is, then

$$\Delta d = \sqrt{\Delta d^2_{sweep} + \Delta d^2_{pol} + \Delta d^2_{\Delta T} + \Delta d^2_{disp}} = 215\,\mu m. \tag{7}$$

3. Preliminary experimental results.

In this Section we report some very preliminary experimental results concerning the *EPR* measurements. The main objective of these measurements is to verify that the experimental method provides accurate measurements of the *EPR* correlations with very small acquisition times of the coincidences. As shown in the Introduction, the presence of superluminal communications can be detected looking at the time dependence of the two correlation parameters S_{max} and S_{min}. Counts N_A and N_B of photons transmitted by polarizers P_A and P_B are detected and back-ground counts due to unwanted external light and to dark noise of the detectors are subtracted. Furthermore, the statistic spurious coincidences $N_{sp} = N_A N_B \delta' t$ are subtracted from the measured coincidences, where $\delta' t$ denotes the pulse duration $\delta' t = 25$ ns of the output pulses generated by the photon counting modules. Numbers $N(\alpha_A, \alpha_B)$ of the measured coincidences that appear in the expressions of the correlation parameters S_{max} and S_{min} are affected by the time-variations of the transmission coefficients in the two arms. The main causes of a variation of the transmission coefficients are: the occurrence of residual displacements of the transmitted beams that are not completely eliminated by the feedback method that reduce the collection efficiency of the entangled photons; the variation of the air relative humidity that induces a change of the light adsorption. In fact, counts $N_A(\alpha_A)$ and $N_B(\alpha_B)$ and coincidences $N(\alpha_A, \alpha_B)$ are related to the transmission coefficients according to

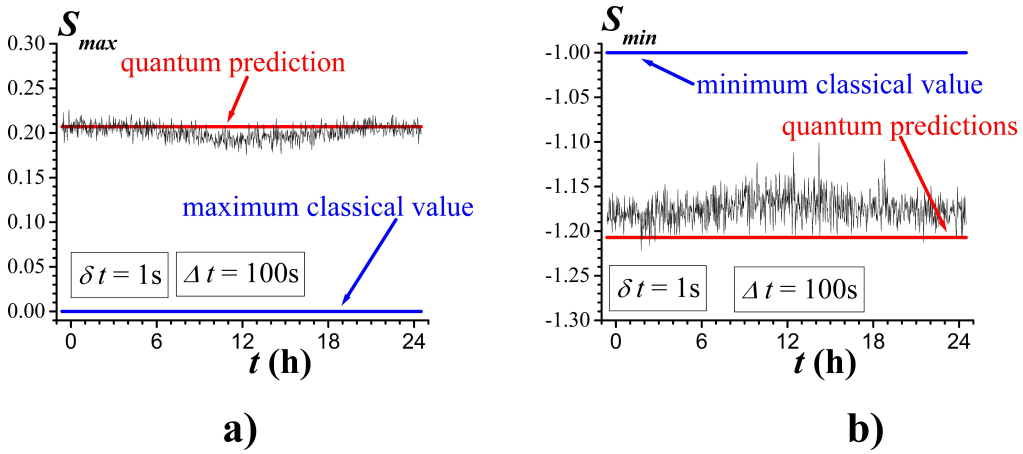

Figure 9: (a): Correlation parameter S_{max} versus the sidereal time. The full red line indicates the dependence predicted by Quantum Mechanics, whilst the blue lower line represents the maximum value allowed by local models of *QM*. (b): The same dependence but for the other parameter S_{min}. Note that parameter S_{min} is much more noisy because it is more sensitive to fluctuations of the coincidences numbers. Note the presence of a systematic effect of the sunlight in the interval between 9 h and 18 h.

relations (8):

$$\begin{aligned} N_A(\alpha_A) &= N\tau_A(\alpha_A)\epsilon_A(\alpha_A)p_A(\alpha_A) \\ N_B(\alpha_A) &= N\tau_B(\alpha_B)\epsilon_B(\alpha_B)p_B(\alpha_B) \\ N(\alpha_A,\alpha_B) &= N\tau_A(\alpha_A)\epsilon_A(\alpha_A)\tau_B(\alpha_B)\epsilon_B(\alpha_B)p(\alpha_A,\alpha_B) \end{aligned} \tag{8}$$

where N is the number of generated entangled photons, $\tau_A(\alpha_A)$ and $\tau_B(\alpha_B)$ are the transmission coefficients, $\varepsilon_A(\alpha_A)$ and $\varepsilon_B(\alpha_B)$ are the efficiencies of photon counting detectors, $p_A(\alpha_A)$ and $p_B(\alpha_B)$ are the probabilities that photons a and b pass through polarizers P_A and P_B (they are $p_A(\alpha_A) = p_B(\alpha_B) = 1/2$ for the entangled state) and $p(\alpha_A,\alpha_B)$ is the joint probability. We see that dividing the coincidences counts $N(\alpha_A,\alpha_B)$ for the product $N_A(\alpha_A)N_B(\alpha_B)$ and multiplying for the product of the average values of $\bar{N}_A(\alpha_A)$ and $\bar{N}_A(\alpha_A)$ one obtains a coincidences number that is no more affected by changes of the transmission coefficients and of the photodetectors efficiencies. Here below we will indicate by $N(\alpha_A,\alpha_B)$ the coincidences corrected according to the procedure outlined above. The correlations parameters S_{max} and S_{min} are obtained repeating measurements of coincidences $N(\alpha_A,\alpha_B)$ with the proper values of angles α_A and α_B that appear in equations (2) and (3). According to equations (2) , (3) and (4), 12 different couples of values α_A and α_B have to be selected rotating the motorized polarizers P_A and P_B. The rotations of polarizers P_A and P_B are controlled by a PC through a labview program that operates in this way: a couple of angles α_A and α_B is set (for instance the first angles 45° and 67.5° of the first contribution in equation (2)), then the polarizers axes are rotated until they reach the setted angles. The corresponding numbers of coincidences $N(\alpha_A,\alpha_B)$ in the acquisition time δt are measured. Then, angles are changed according to equations (2), (3) and (4) and the corresponding values of the coincidences are measured. When all the 12 values of coincidences that are needed to calculate parameters S_{max} and S_{min} have been measured, the labview program calculates these correlation parameters. Unfortunately, the average time that is needed to rotate the polarizers is of the order of 8 seconds and, thus, the duration of a single measurement of S_{max} and S_{min} requires a time $\Delta t \approx 100\,\mathrm{s}$ that is much larger than the acquisition time δt of coincidences. Then, the maximum superluminal velocity $\beta_{t,min}$ that can be detected in the present experiment is not limited by the acquisition time δt of the coincidences but by the much larger effective acquisition time $\Delta t = 100$ s. Figures 9a) and 9b) show the

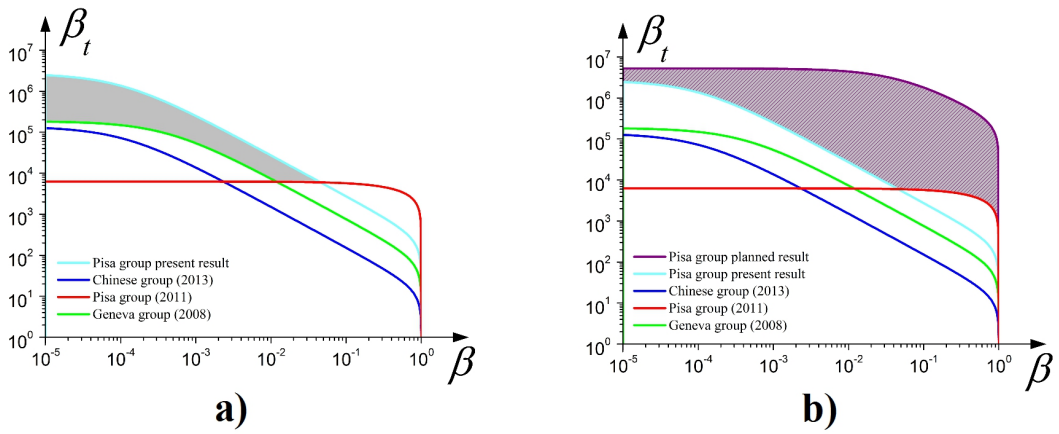

Figure 10: (a): The reduced superluminal velocity β_t versus the reduced velocity β of the preferred frame. The curves in the figure represent the lower bounds $\beta_{t,min}$ that have been established in the previous experiments and in the present one. The filled region represents the new region of superluminal velocities that are investigated here. (b) The filled region represents the new region of superluminal velocities that should be explored in the final experiment with the acquisition time $\delta t = 0.1$ s.

values of the correlation parameters S_{max} and S_{min} versus time during a sidereal day when the coincidences acquisition time was δt =1 s but the effective acquisition time was $\Delta t = 100$ s. The full horizontal lines in figures 9a) e and 9b) correspond to the prediction of QM and to the maximum (figure 9a)) and minimum (figure 9b)) values allowed by local theories. According to the Introduction, parameter S_{max} would become lower than 0 and S_{min} would become greater than - 1 at two times each sidereal day if the superluminal signals have velocities lower than $\beta_{t,min}$. This behaviour is not observable in figures 9a) and 9b) and, thus, we can conclude that, if superluminal signals are responsible for QM correlations, then the superluminal velocities are greater than the maximum measurable values ($\beta_t > \beta_{t,min}$). The results in figures 9a) and 9b) were obtained using the coincidences acquisition time $\delta t = 1$ s but we have verified that sufficiently accurate results are also obtained using the much smaller acquisition time $\delta t = 0.1$ s where the relative statistical noise increases by a factor $\sqrt{10}$. Notice that parameter S_{min} exhibits much greater fluctuations than S_{max} and, thus, this latter parameter provides a much more accurate test of the EPR correlations. This behaviour is probably due to the fact that the absolute value of S_{max} is about six times lower than that of S_{min}. For this reason the planned final measurements will be made using the S_{max} parameter alone that is affected by a much smaller noise. Furthermore, it is important to remark that the measurements shown in figures 9a) and 9b) were obtained in a July day (30 July 2016) with very strong sunlight. The residual noisy effects due to sunlight are evident looking at the experimental points between times t = 9 h and t = 18 h in the figures. All these effects are absent in conditions of fully covered sky.

Substituting the effective acquisition time $\Delta t = 100$ s in place of δt in equation (6) with the uncertainty $\Delta d = 215\,\mu$m, we obtain the lower bound $\beta_{t,min}$ that corresponds to our preliminary results. In figure 10 a) we show the lower bounds already found in some previous experiments [28–30] together with that obtained here. The filled region represents the new region of superluminal

velocities investigated here. In figure 10 b) we show also the planned values of $\beta_{t,min}$ that should be obtained in our final experiment with a 0.1 s effective acquisition time. The filled region in figure 10 b) corresponds to the new region of superluminal velocities that will become accessible in the final experiment. The experimental method that will be used to bypass the problems related to the polarizers movement will be briefly outlined in the Conclusions below.

4. Conclusions

In the present paper we have developed an accurate and stable method to equalize the optical paths of the entangled photons over a kilometric distance. Due to vertical gradients of the air refractive index in the *EGO* gallery induced by sunlight it has been needed to greatly modify the experimental apparatus proposed in[27] introducing a complex feedback procedure to correct the deviations of the beams and the astigmatism of the images. In such a way we were able to obtain two virtually stable 1:1 images of the source of entangled photons at the centre of two polarizers lying at a distance of ≈ 600 m from the source. This ensures that virtually all the entangled photons transmitted by the polarizers are collected by the photon counting detectors also in the unfavourable conditions of maximum sunlight. The interference method used to equalize the optical paths exploits two reference beams reflected by the polarizers. The reference beams follow the average paths of the entangled photons. The method to produce the reference beam has been greatly improved with respect to the original project[27] thanks to the use of a suitable optical grating. The new method automatically ensures that the reference beams are superimposed to the entangled ones and that they have the same phase at the *BBO* plates without using the complex equalization procedure outlined in our original paper[27]. Finally, a suitable design of the optical components and the use of the compensation procedure developed by the Kwiat group[33–35] provides a great number of measured coincidences and makes possible to use a very short acquisition time $\delta t = 0.1$ s. Using this experimental apparatus we have continuously measured the correlation parameters S_{max} and S_{min} for an entire sidereal day to obtain some very preliminary results. Our experimental results are greatly affected by the long time that is needed to rotate the polarizers that leads to an effective acquisition time $\Delta t = 100$ s much greater than the minimum acquisition time of coincidences $\delta t = 0.1$ s. For this reason, the new explored region of the velocities of the superluminal signals investigated here (see figure 10 a)) is much smaller than the planned one (see figure 10 b)). Due to the strong vertical temperature gradients it has not been possible to perform the experiment along the true East-West direction that was proposed in our previous paper. In the present experiment the measures have been performed in the so called "East-West" gallery of *EGO* that makes the angle $\gamma = 18°$ with the actual East-West axis. Then, only a 95% portion of the celestial sphere is accessible with our experimental apparatus.

In order to become insensitive to the long time needed to rotate the polarizers and to reach an effective acquisition time $\delta t = 0.1$ s, it is needed to fully change the acquisition method. With this improved method we should obtain the planned results in figure 10 b). Here we describe only the main idea of the new method. Using a NTP+PTP GPS Network Time Server (TM2000A) and knowing the values of the difference *UTC-UT1* provided in the Web by *IERS* [37] we will be able to synchronize the measurements of the coincidences with the Earth rotation angle with respect to the fixed stars within a few milliseconds uncertainty. That accurate synchronization of the measurements cannot be obtained using a *PC* but requires the use of a real time acquisition. This will be obtained using a *Compact DAQ* (National Instruments 9132) in place of the *PC* to acquire the coincidences and a Real Time Labview program to control any aspect of the acquisition. In this way, will be possible to acquire the coincidences in successive days at the same Earth rotation times. The measurement method will follow the steps below: i) the real time labview program rotates polarizers to reach the angles α_A and α_B that correspond to the first contribution $N(45°, 67.5°)$ in the expression of S_{max} in equation (2). ii) When the Earth

rotation angle reaches a well defined value, the acquisition of coincidences starts and 2^{20} values of coincidences are acquired in a full Earth rotation day. The successive day, the real time labview program sets the polarizers angles to the values corresponding to the second term in the expression of S_{max} and the acquisition of coincidences will start with sidereal synchronism with the measurements of the previous day. The same procedure will be repeated until all the contributions that are present in the expression of S_{max} have been obtained. With this procedure, the effective acquisition time coincides with the coincidences acquisition time δt and the planned region of superluminal velocities (filled region in figure 10 b)) should become accessible. If the revolution motion of the Earth around the Sun and the precession and nutation of the Earth axis would be absent, the losses of quantum correlations should occur exactly at the same earth rotation angles each sidereal day and, thus, one could utilize the coincidences $N(\alpha_A, \alpha_B)$ measured in successive days at the same earth rotation angles to calculate the time dependence of the correlation parameter S_{max} using equations (2) and (4). Unfortunately, the analysis of the experimental data will be much more complex due to the revolution motion of the earth around the Sun and to the precession and nutation motions. In fact, the losses of quantum correlations should occur when the relative velocity $\vec{V}$ of the preferred frame with respect to the Earth frame becomes orthogonal to the A-B axis. Due to the revolution motion of the earth around the Sun and to the precession and nutation motions, the angle between the relative velocity $\vec{V}$ of the preferred frame and the A-B axis is not a true periodic function having the period of the Earth rotation and, thus, the orthogonality condition will be not exactly satisfied at the same Earth rotation angles in different days. Then, the analysis of the experimental results will need more complex procedures that will be not discussed here.

Acknowledgements
We acknowledge Marco Bianucci for the realization of many electronic devices and for a great number of helpful and fundamental suggestions. We also thank the European Gravitational Observatory of Cascina (Italy) that host our experiment and, in particular, the director Federico Ferrini and Franco Carbognani and Stefano Cortese for their valuable support and for their kindness. We also thank the Istituto di tecnologie della comunicazione, dell'informazione e della percezione (S. Anna) for giving us two LCM1555EW4932-64 0f Nortel Networks. This work was supported by La Fondazione Pisa.

References

[1] Einstein A, Podolsky B and Rosen N 1935 *Phys. Rev.* **47**(10) 777–780
[2] Gisin N 2014 *Quantum Correlations in Newtonian Space and Time: Faster than Light Communication or Nonlocality* (Milano: Springer Milan) pp 185–203 URL `http://dx.doi.org/10.1007/978-88-470-5217-8_12`
[3] Gisin N 2014 *Quantum Chance - Nonlocality, Teleportation and Other Quantum Marvels* (Springer International Publishing)
[4] Bell J S 1964 *Physics* **1** 195–200
[5] Freedman S J and Clauser J F 1972 *Phys. Rev. Lett.* **28**(14) 938–941
[6] Aspect A, Dalibard J and Roger G 1982 *Phys. Rev. Lett.* **49**(25) 1804–1807
[7] Zeilinger A 1986 *Phys. Lett.* A **118** 1–2
[8] Tittel W, Brendel J, Zbinden H and Gisin N 1998 *Phys. Rev. Lett.* **81**(17) 3563–3566
[9] Weihs G, Jennewein T, Simon C, Weinfurter H and Zeilinger A 1998 *Phys. Rev. Lett.* **81**(23) 5039–5043
[10] Aspect A 1999 *Nature* **398** 189–190
[11] Pan J, Bouwmeester D, Daniell M, Weinfurter H and Zeilinger A 2000 *Nature* **403** 515–519
[12] Grangier P 2001 *Nature* **409** 774–775

[13] Rowe M A, Kielpinski D, Meyer V, Sackett C A, Itano W M, Monroe C and Wineland D J 2001 *Nature* **409** 791–794

[14] Matsukevich D N, Maunz P, Moehring D L, Olmschenk S and Monroe C 2008 *Phys. Rev. Lett.* **100**(15) 150404

[15] Davies P C W and Brown J R 1993 *The ghost in the atom: a discussion of the mysteries of quantum physics* canto ed. ed (Cambridge; New York: Cambridge University Press)

[16] Eberhard P H 1989 A realistic model for quantum theory with a locality property *Quantum theory and pictures of reality: foundations, interpretations, and new aspects* ed Schommers W (Berlin; New York: Springer-Verlag)

[17] Bohm D and Hiley B J 1991 *The undivided universe: an ontological interpretation of quantum mechanics* (Routledge)

[18] Møller C 1955 *The theory of relativity* (Oxford: Clarendon)

[19] Kowalczyński J 1984 *Int. J. Theor. Phys.* **23**(1) 27–60

[20] Reuse F 1984 *Ann. Phys.* **154** 161–210

[21] Caban P and Rembieliński J 1999 *Phys. Rev.* A **59**(6) 4187–4196

[22] Maudlin T 2001 *Quantum non-locality & relativity* (Oxford: Blackwell)

[23] Cocciaro B 2013 *Physics Essays* **26** 531–547

[24] Bancal J, Pironio S, Acín A, Liang Y, Scarani V and Gisin N 2012 *Nat. Phys.* **8** 867–870

[25] Barnea T J, Bancal J D, Liang Y C and Gisin N 2013 *Phys. Rev. A* **88**(2) 022123

[26] Aspect A 2002 Bell's theorem: The naive view of an experimentalist *Quantum (Un)speakables: From Bell to Quantum Information* ed Bertlmann R A and Zeilinger A (Springer)

[27] Cocciaro B, Faetti S and Fronzoni L 2013 *Journal of Physics: Conference Series* **442** 012005

[28] Salart D, Baas A, Branciard C, Gisin N and Zbinden H 2008 *Nature* **454** 861–864

[29] Cocciaro B, Faetti S and Fronzoni L 2011 *Phys. Lett.* A **375** 379–384

[30] Yin J, Cao Y, Yong H L, Ren J G, Liang H, Liao S K, Zhou F, Liu C, Wu Y P, Pan G S, Li L, Liu N L, Zhang Q, Peng C Z and Pan J W 2013 *Phys. Rev. Lett.* **110**(26) 260407

[31] The Virgo collaboration 1997 *Final Design Report* (Virgo Technical Note VIR-TRE-DIR-1000-13)

[32] Kwiat P G, Waks E, White A G, Appelbaum I and Eberhard P H 1999 *Phys. Rev. A* **60**(2) R773–R776

[33] Altepeter J, Jeffrey E and Kwiat P 2005 *Opt. Express* **13** 8951–8959

[34] Akselrod G M, Altepeter J B, Jeffrey E R and Kwiat P G 2007 *Opt. Express* **15** 5260–5261

[35] Rangarajan R, Goggin M and Kwiat P 2009 *Opt. Express* **17** 18920–18933

[36] Ciddor Equation URL `http://emtoolbox.nist.gov/wavelength/ciddor.asp`

[37] International Earth Rotation and Reference Systems Service URL `https://www.iers.org/IERS/EN/Publications/Bulletins/bulletins.html`